A Conceptual Design Optimization for a MgB2 DC Transmission Line

A conceptual design optimization for a MgB_2 DC transmission line

Andrea Musso, Lorenzo Cavallucci, Giuliano Angeli, Marco Bocchi and Marco Breschi

***Abstract* — This work presents a tool to define an optimized architecture of DC superconducting cables realized with magnesium diboride (MgB_2), aimed at minimizing the cable system costs by determining the optimal values of the geometric, physical, and operating parameters. The methodological approach is implemented in the numerical tool OSCaR, previously developed for HTS AC coaxial cables, and adapted here to the analysis of MgB_2 conductors. The major updates to the original code are listed in a dedicated section of this manuscript. As an upgrade of the previous version of the model, the fluid-dynamic constraints are evaluated with an accurate modeling of the thermodynamic and thermophysical properties of the cryogenic fluid. Helium gas is selected as the cable cryogen, but the tool allows the user to select also other cryogenic fluids (*e.g.* liquid hydrogen). As an example of the flexibility of the proposed tool, the results of a parametric analysis are provided. The optimized costs of the cable system, distinguishing between several cost indexes, and some optimized individual design parameters of the MgB_2 line are presented as a function of the delivered power.**

***Index Terms* — Superconducting cables, MgB_2 conductors, Transmission lines, Techno-economic optimization.**

I. Introduction

The application of magnesium diboride (MgB_2) to high-power transmission lines has long been considered [1], and the interest has recently been reinvigorated by the European BEST PATHS project [2], the Superconducting Link project at CERN [3] and cable prototype realized at the JSC VNIIKP Institute (Russia) [4]. Given its relatively low manufacturing cost compared to High Temperature Superconducting (HTS) tapes and a critical temperature compatible with liquid hydrogen, MgB_2 would be a good candidate for realizing transmission lines transporting both electric and chemical energy from renewable offshore plants [5, 6, 7, 8, 9]. To reduce the consumption of expensive cryogenics, the proposed use is generally limited to DC lines [10, 11], but improvements to wires and cables design to apply MgB_2 also for AC lines are investigated [12, 13]. However, for this technology to take hold in the market, the possible scenarios of techno-economic convenience compared to conventional cables (or other superconducting options) must be identified. To date, a poor number of case studies and cost analyses of superconducting cables are available, considering limited conductor and operating parameters [14, 15, 16, 17, 18, 19, 20, 21], very few of them referred to MgB_2 cables [22].

This work describes a techno-economic optimization tool for MgB_2 DC cables consisting of two-way lines with a single cryogen flow and adopting the so-called *both-sided cooling option*. The methodology is adapted from the tool called OSCaR (Optimization tool for Superconducting Cable Research) [23], originally developed for triaxial HTS AC coaxial cables [24]. The main modifications imposed to the original algorithm to parametrize costs, losses and design factors referred to DC MgB_2 cables are reported. Finally, some examples of parametric analyses obtained with the proposed tool are provided, to identify cost trends and assist in defining design choices.

This work was financed by the Research Fund for the Italian Electrical System under the Three-Year Re-search Plan 2022-2024 (DM MITE n. 337, 15.09.2022), in compliance with the Decree of April 16th, 2018. *(Corresponding author: A. Musso. Contact: andrea.musso@rse-web.it).*

Andrea Musso, Giuliano Angeli and Marco Bocchi are with RSE S.p.A., 20134 Milan, Italy.

Lorenzo Cavallucci and Marco Breschi are with the Department of Electrical, Electronic and Information Engineering 'Guglielmo Marconi' of the University of Bologna, 40126 Bologna, Italy.

Color versions of one or more figures in this article are available at https://doi.org/...

II. Description of the Optimization Method

The proposed tool determines the optimized cable design according to the operating parameters selected by the user, corresponding to the lowest system cost. A constrained minimization problem for a multi-variable function is solved using a genetic algorithm implemented in MATLAB [25]. Specifically, the total cost of a MgB_2 cable system (C_{tot}) is minimized, defined as:

$$C_{tot} = C_{MgB_2} + C_{ins} + C_{cool_{cap}} + C_{vac} + C_{cryo} + C_{He} + \\ + C_{Cu} + C_{ter} + C_{cab} + C_{lay} + C_{cool_{op}} + C_{man} + C_{dis} \quad (1)$$

where the cost indexes in (1) are parameterized to the specific design choices, distinguishing between capital and operating costs. Capital costs combine the cost of MgB_2 wires (C_{MgB_2}), the electrical insulation material (C_{ins}), the development and installation of cooling/pumping stations ($C_{cool_{cap}}$), the vacuum system (C_{vac}), the cryostat (C_{cryo}), the amount of helium contained in the closed loop cryogenic system used to cool down the cable (C_{He}), the copper necessary for the cable former and shield (C_{Cu}), the electric terminations (C_{ter}), the cabling costs (C_{cab}), and the laying costs (C_{lay}). The operating costs includes the electric energy needed to operate the cooling/pumping stations ($C_{cool_{op}}$), and the costs for cable maintenance (C_{man}) and dismantling (C_{dis}).

The thermal inputs from the cryostat and the heat generated by the cable components are computed for all configurations during the optimization process. Constraints are imposed on the maximum and minimum current that can be transported by the MgB_2 wires and on the pressure and temperature limits that can

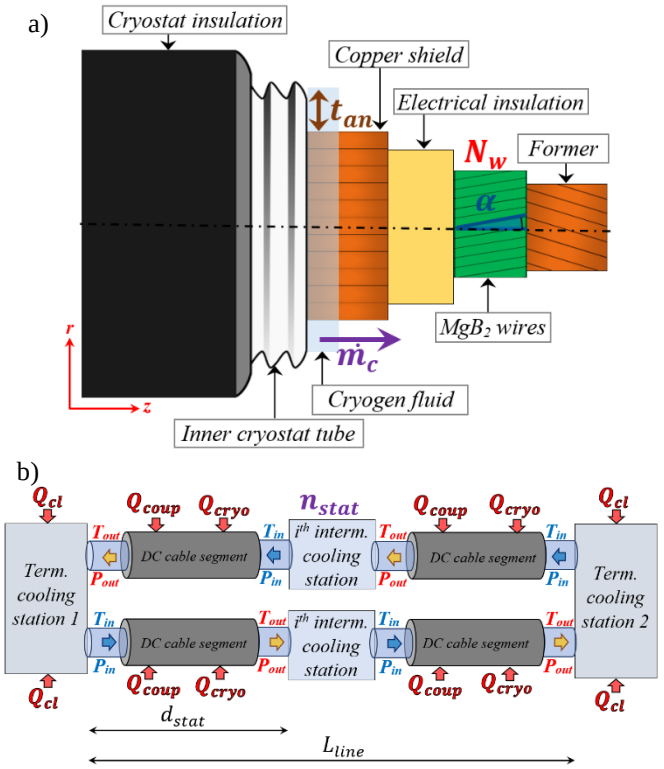

Fig. 1. (a) Sketch of the lateral view of a DC MgB_2 cable, not in scale. The bold terms refer to some of the design parameters modified throughout the optimization process. (b) Sketch of the both-sided cooling option with a single intermediate cooling station per way. The bold red terms indicate the heat inputs to the cable segments and to the cooling stations.

be reached by the cryogenic fluid (helium gas or liquid hydrogen) in a cable segment. An exhaustive mathematical description of the model is reported in [24], referred to AC coaxial HTS cables. Only the main modifications to the model equations implemented to study MgB_2 DC cables are reported here. Thus, all input parameters not explicitly mentioned in this work are the same as adopted in [24].

A.MgB₂ cable design and electrical considerations

Fig. 1a shows a sketch of the lateral view of the cable design. Among the different architectures that have been proposed in the literature for MgB_2 DC cables [1, 2, 3, 4, 26], the design proposed in [6] is selected, assuming the various layers to be concentric. However, the proposed methodology can be applied to cables with double cryostats/fluids, as well as multi-petal layouts. The cable is composed of a copper former, supporting the MgB_2 wires. Differently from the approach presented in [24], the radius of the former (R_f) is no longer a problem variable, but it is computed from the number of MgB_2 wires (N_w). The latter is instead added to the optimizable parameters (bold terms in Fig. 1a). Each algorithm step starts with a N_w value selected between the upper and lower boundaries imposed by the user. Then, the radius R_f is computed to arrange all the MgB_2 wires around the corresponding former circumference, leaving no space between adjacent wires. The wires are wound with a winding angle α, ranging from 7° to 15° due to practical mechanical limits. The angle affects the total length of MgB_2 wires required to wind the cable and the losses due to current ripples. The electrical insulation thickness necessary to withstand the nominal cable voltage is calculated with the methodology described in [21]. This work considers laminated polypropylene paper (PPLP) as an insulating material; the breakdown strength of 85 kV/mm has been selected as an average of the values found in [27, 28, 29, 30, 31, 32, 33, 34]. Then, the insulator is surrounded by a copper stabilizer shield, whose thickness is calculated to obtain the same amount of copper as in the former [21].

B.Hydraulic and cooling considerations for the MgB₂ cable

The concentric layers are contained within an annular duct of optimizable thickness t_{an}, where the cryogenic fluid flows with a mass flow rate $\dot{m}_c$. Thus, the cable design can be classified among the *Cold Dielectric* ones, like most of the superconducting cables prototypes recently proposed. Finally, the cable is contained within a 20 mm thick cryostat. Note that Fig. 1a does not show very thin layers: a 1.9 mm thick levelling layer is interposed between the former and the MgB_2 wires [35], a 0.36 mm thick carbon black layer is interposed both between the MgB_2 wires and the insulation and between the insulation and the copper shield, and a 0.3 mm thick core fixture layer is interposed between the copper shield and the annular duct.

Fig. 1b shows a sketch of the cable system coupled to its cooling apparatus. The so-called *both-sided cooling option* is adopted in this work [35], resulting in a termination cooling station at each cable end. Then, each cable segment is included between a pair of cooling stations. Each cooling station must re-establish the initial temperature and pressure conditions (T_{in} and P_{in}) of the input cryogen (orange arrows) before pumping it into the following cable segment (blue arrows), by compressing it and removing the heat it absorbed along the length of the previous segment. To avoid exceeding the user-imposed constraints on the maximum temperature rise (ΔT_{max}) and pressure drop (ΔP_{max}), a number of intermediate cooling stations n_{stat} can be present along the line length (L_{line}). In this work, the cable is refrigerated with helium gas, entering each segment at T_{in} = 20 K and P_{in} = 20 bar and imposing ΔT_{max} = 10 K and ΔP_{max} = 12 bar. However, the tool already considers the properties of 15 alternative cryogenic fluids, that a user can easily select.
For a fair comparison with AC cables, the DC line is designed with one forward and one return conductor, both included between the same pair of termination cooling stations. Finally, as in [24], the cable geometry is assumed to be modular: all cable segments are identical. Thus, it is sufficient to optimize the design of a single segment of length d_{stat}. Furthermore, since the forward and return cables are identical, it is sufficient to estimate the cost of a cable route and then double it.

C.Loss function

Following the sketch presented in Fig. 1b with red arrows, each intermediate cooling station eventually present has to manage a quantity of heat Q_{int}, while each termination cooling station has to handle a quantity Q_{term}, both expressed in (2).

Q_{cryo} is the heat entering from the cryostat, computed as in [24, 36]. Q_{cl} is the heat produced by 2-stage current leads (copper to HTS at 77 K and HTS to MgB_2 at 20 K), calculated as in [21].

$$Q_{int}(T) = Q_{cryo}(T) + Q_{coup}$$
$$Q_{term}(T) = Q_{cryo}(T) + Q_{coup} + 2Q_{cl} \quad (2)$$

Note that each termination station has to manage the thermal power Q_{cl} coming from the "inlet" termination of the forward cable and from the "outlet" termination of the return cable. Q_{coup} are the losses produced in the MgB_2 wires due to the AC ripples at pulsation ω, which are eventually superimposed to the DC transport current. The calculation of the coupling losses was performed according to [37]. In the model, the power along a cable segment d_{stat} is computed as:

$$Q_{coup} = \frac{B_m^2}{4\mu_0}\frac{\tau\,\omega^2}{(\tau^2\omega^2+1)}\frac{d_{stat}\,N_w\,\pi\,R_w^2}{\cos(\alpha)} \quad [\mathrm{W}] \quad (3)$$

where B_m is the field amplitude due to the current ripple superimposed to the DC current [38], τ is the cable time constant computed as a function of the twist pitch [37] and R_w is the radius of the MgB_2 wires.

D. I_c parametrization and magnetic field estimation

In this work, a MgB_2 wire with characteristics similar to those produced by ASG Superconductors S.p.A. is adopted [39, 40], but the user can freely analyze different conductors. The wire diameter is set to 1.33 mm. The I_c dependence on temperature and field is taken into account by means of a simple parametrization. The temperature of the MgB_2 wires is assumed equal to that of the cryogen at the same cross-section; the magnetic field applied to the wires is computed with an analytical formulation [41] under the assumption of a uniform current distribution over the annular section enclosing the wires.

E.Constraint on the operating current of each MgB_2 wire

It is assumed that I_{op} redistributes equally among the MgB_2 wires. The ratio between the current in each wire and their minimum I_c along a cable segment (*i.e.* the one corresponding to the most heated location) is bound to range between a minimum value (here 55%), not to excessively underload the wires, and a maximum safety value (here 75%). Eventually, if the contribution to the costs given by the superconductor is not dominant, it may result economically advantageous to underload the wires, increasing N_w but reducing other related cost indexes.

F. New fluid-dynamic modelling

A relevant upgrade compared to the previous version of the model concerns the fluid-dynamic constraints, here evaluated with a mathematical modeling of all the thermodynamic and thermo-physic properties of the cryogenic fluids. This approach is more accurate than the analytical formulae used in [24] to estimate ΔT_{max} and ΔP_{max}. It was originally proposed in [42] and it has been revised for the topic of this work. The model has been validated by comparing its results with those of an equivalent code [43], for the same case studies and cryogenic fluids.

The final non-linear differential equations system in (4) is obtained from the equations of energy and momentum conservation and the continuity equation, considering stationary conditions, and applying a 1-dimensional (the cable length *x*) approximation. The system parameters are detailed in (5 - 6).

$$\begin{bmatrix}\frac{\partial T}{\partial x}\\ \frac{\partial \rho}{\partial x}\end{bmatrix} = \left[Q_{\delta T\delta\rho}(\rho,T)\right]^{-1}\begin{bmatrix}-\int_0^{d_{stat}}\left[Q_{cryo}(T)+Q_{coup}\right]a_c\,dx - \frac{\dot{m}_c\,\tau_c\,p_c}{a_c^{\,2}\,\rho}\\ \dot{m}_c\,g\,\sin\beta + \frac{\dot{m}_c\,\tau_c\,p_c}{a_c^{\,2}\,\rho}\end{bmatrix} \quad (4)$$

$$\left[Q_{\delta T\delta\rho}(\rho,T)\right]^{-1} = \frac{1}{\Delta Q_{\delta T\delta\rho}(\rho,T)}\begin{bmatrix}G_{\delta\rho}(\rho,T) & -H_{\delta\rho}(\rho,T)\\ -G_{\delta T}(\rho,T) & H_{\delta T}(\rho,T)\end{bmatrix} \quad (5)$$

$$\Delta Q_{\delta T\delta\rho}(\rho,T) = H_{\delta T}(\rho,T)G_{\delta\rho}(\rho,T) - G_{\delta T}(\rho,T)H_{\delta\rho}(\rho,T)$$

$$H_{\delta T} = \frac{\dot{m}_c}{a_c\,\rho}\left(\frac{\partial P}{\partial T} - \rho\frac{\partial h}{\partial T}\right)\ ;\ H_{\delta\rho} = \frac{\dot{m}_c}{a_c\,\rho}\left(\frac{\partial P}{\partial \rho} - \rho\frac{\partial h}{\partial \rho}\right)$$
$$G_{\delta T} = -\frac{\dot{m}_c}{a_c\,\rho}\frac{\partial P}{\partial T}\ ;\ G_{\delta\rho} = \frac{\dot{m}_c}{a_c\,\rho}\left(\frac{\dot{m}_c^{\,2}}{\rho^2} - \frac{\partial P}{\partial \rho}\right) \quad (6)$$

where p_c and a_c are the perimeter and cross-section of the portion of the duct involved in the flowing of coolant. g is the gravity acceleration and β is the slope of the duct. τ_c is the shear stress due to the friction between the fluid and the cryostat walls, calculated as in [42]. The derivatives of the specific enthalpy (h) and the pressure in (6) are computed in agreement with [44, 45]. Unlike Q_{cryo} and Q_{coup}, Q_{cl} is not included in the heat input to the fluid in (4) since it is managed by a dedicated cooling system.

The system in (4) has to be solved numerically to compute the cryogen temperature and density ρ at different locations of a cable segment. The use of density and temperature as state variables, rather than the more common pressure and temperature, is a consequence of the adopted formulation for the thermodynamic and thermo-physic properties of the fluids, as outlined in [44, 45]. These properties and their derivatives are expressed analytically as functions of density and temperature. Having selected this approach, the pressure is derived once the system in equation (4) is solved.

The details of this treatment, here omitted for reasons of space, may be the subject of future publications.

G.Updated cost parameters and indexes

Several cost indexes have been updated to consider the new cable design and components. These terms are described in the following and summarized in Table I. Following the nomenclature in [24], when a cost index is expressed with the uppercase letter (C) it indicates the total cost, while the use of a lowercase

TABLE I
UPDATED COST PARAMETERS AND INDEXES

Parameter	*Unit*	*Value*	*Reference*

c_{MgB_2}	€/m	2	Mean of values in [21, 22, 46]
c_{cryo}	M€/km	1.5	Mean of values in [22, 46]
$c_{cryocooler}$	k€/kW	200	[21]
c_{cab}	M€/km	1.5	Halved from the value in [24]
c_{He}	€/liter	12	[22]
c_{Cu}	€/kg	7.5	[49]
$C_{cool_{fixed}}$	k€	400	Doubled from the value in [24]
C_{ter} (each way)	k€	400	[47]

letter (c) represents the unitary cost.

The cost of a MgB_2 wire (c_{MgB_2}) is set to 2 €/m, as an average of the values in [21, 22, 46].

The unit cost of the cryostat (c_{cryo}) has been significantly increased over that used for a liquid nitrogen cooled cable [24], as it is expected to feature higher performing (and expensive) materials to handle helium or hydrogen; a cost of 1.5 M€/km has been selected as a mean of the values reported in [22, 46]. The capital cost per unit of power of each cooling station ($c_{cryocooler}$) has been increased from 100 k€/kW to 200 k€/kW, in agreement with [21]. The additional fixed costs required for each cooling station ($C_{cool_{fixed}}$) besides the device cost (installation, maintenance, and disposal) has been increased to 400 k€, considering the more challenging fluids to handle compared to liquid nitrogen.

The termination costs are set equal to 400 k€ for each cable way, as an average of the 2-stage termination costs in [47].

The unitary cabling cost (c_{cab}) is halved compared to the value set for AC coaxial HTS cables [24] which corresponded to 3 M€/km. In fact, a DC cable design does not require three insulated concentric phases, and handling MgB_2 wires instead of HTS tapes is expected to be cheaper.

The cost of helium gas (c_{He}) is assumed to be 12 €/liter [22], while the cost of the alternative liquid hydrogen is 7.5 €/kg [48].

Moreover, a new cost index is added to the capital costs, not adopted in [24]. It accounts for the cost of the copper required for the former and the shield (C_{Cu}). A cost of 7 €/kg is selected for the copper (c_{Cu}), from market price at the time of submission [49]. Note that in this work, the filling factor possibly present between the copper strands composing the former and the shield is neglected as they are both considered as solid volumes. This approximation is considered reasonable given the low impact of copper on the total capital cost, which is also omitted from the figures in Section III for reasons of space.

Finally, (7) reports how to compute the power required by the pump present in the k^{th} cooling/ pumping station to restore the cryogen pressure (Q_{p_k}), whose corresponding energy in the considered time interval then contributes to the operating cost term $C_{cool_{op}}$.

$$Q_{p_k} = \dot{m}_c \, \Delta P / \rho \tag{7}$$

The equation has been adjusted from [24], to consider the *single coolant flow* case analyzed in this work. Differently from the case of two counter-flows of coolant, there is no need to distinguish between the power required to handle the two distinct flows, as a single ΔP is present.

III. Results of the techno-economic analysis

As an example of the tool flexibility, the results of a parametric analysis performed by varying the power transmitted by a DC cable are presented. A two-way 10 km long line is considered, operating at a voltage level of 220 kV. The MgB_2 cable is cooled with helium gas. With the exception of the new/updated cost indexes described in Section II.G, the remaining cost parameters are the same used for the OSCaR tool, listed in [24].

Fig. 2a shows the capital costs per kilometer of cable, for the combination of cases analyzed. Note that all the costs, except those referred to the termination cooling stations, are doubled as the line is composed by a forward and a return cable. It is evident that cryostat and cabling costs are the largest contributors to the capital costs. However, they are considered constant per unit of cable length, and thus have a limited impact on the optimization process. It is possible that the parameters entered are too conservative compared to the real capabilities of a cable manufacturer. In the future, these indexes could be updated, be the subject of dedicated parametric analyzes, or be computed differently. Then, the cost of MgB_2 rises as the power increases, as N_w grows from 15 to 32 and the winding angle does not decrease; thus, the total length of MgB_2 wires required rises. However, its impact on total capital costs is very limited (less than 1.5%). Between 1 and 3 GW, the capital cost of cooling stations increases with power, contributing 15% of total capital costs. In fact, they are designed to manage a thermal load that rises with the power delivered by the cable, and therefore require proportionally higher capital investments. Indeed, as shown in Fig. 2b, the total losses generated in one of the two cable ways of the 10 km line grows from 17.1 kW for a 1 GW cable, up to 18.4 kW for a 3 GW cable. The load increase is due to the increment of Q_{cl}, which is proportional to the operating current. This is partially balanced by the reduction of Q_{cryo} with power, ranging between 95% (1 GW) and 86% (3 GW) of the total losses. As regards the coupling losses, they are 4 – 5 orders of magnitude lower than the other contributions, and thus negligible.

Fig. 2c shows the operating costs per kilometer of cable, varying the power. These costs, calculated over a 40-year period, are more than double the capital costs. The operating costs depend solely on the electric energy required for the cooling stations, as dismantling and cabling costs are negligible. Thus, the trend of operating costs is directly proportional to the thermal inputs trend, as well as the pressure drop the pressure/cooling stations must recover, which increases from 3.9 bar to 5.1 bar between 1 GW and 3 GW.

Fig. 2c distinguishes between the costs of the intermediate and termination cooling stations (the latter labeled 1 and 2). The total operating costs of intermediate stations are higher than those of a single termination station since the algorithm proposes to use at least one for each forward or return cable (thus at least two along the 2-way line). Indeed, n_{stat} is equal to 1 between 1 GW and 2 GW, rising to 2 in the 3 GW case.

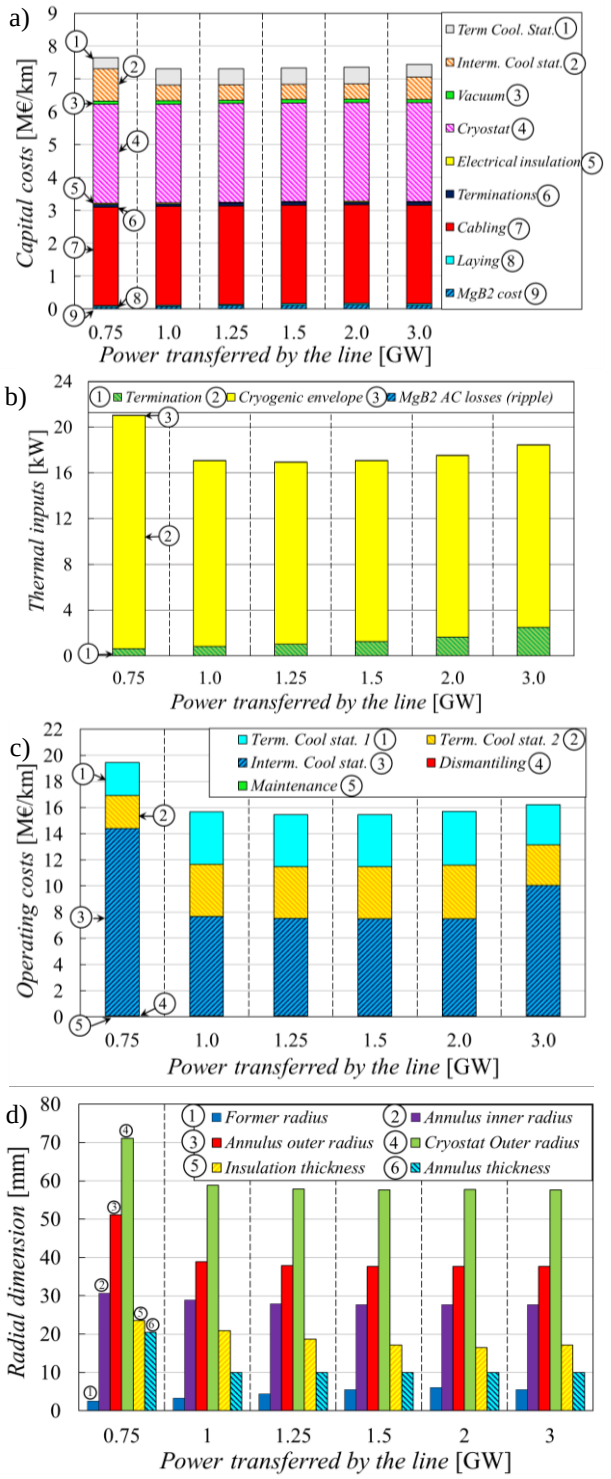

Fig. 2. (a) Capital costs per kilometer of cable. (b) Thermal inputs in one of the two cable ways. (c) Operating costs per kilometer of cable. (d) Radial dimension of the main concentric components of the cable, varying the delivered power. A voltage level of 220 kV and a 10 km long line are considered.

Note that n_{stat} is increased to cope with the increasing losses of Fig.2c while complying the fluid-dynamic constraints, with a threshold trend, given that it can only assume integer values. This growth in n_{stat} leads to a slight reduction in the operating and capital costs of each individual cooling station despite the overall losses in the cable increase. In fact, decreasing d_{stat}, the amount of heat they must handle individually also decreases.

It is worth noting that the results of the 0.75 GW case differ from the cost trends described above, showing higher capital and operating costs than those found for the other power levels. This is essentially due to the optimized cable geometry for this case, whose cryostat radial encumbrance is significantly greater than in the other cases, as shown in Fig. 2d. This is valid despite having assumed the cryostat thickness to be constant (2 cm). In fact, the 0.75 GW case, although starting from a smaller former radius than the other cases, requires both greater thicknesses of electrical insulation and of the annular duct. These thicknesses contribute to increasing the radial encumbrance of the cable and the external surface of the cryostat. In turn, Q_{cryo} increases as the cryostat outer radius increases [24, 36], since the surface area for thermal inputs expands. It follows that the losses of the 0.75 GW case tops 21 kW per cable way (as in Fig. 2b), requiring a greater capital and operating costs for the intermediate cooling stations compared to the other power levels analyzed. Moreover, the 0.75 GW case also has the highest value of n_{stat} (equal to 3) since it has to cope with the higher thermal inputs.

Finally, Fig. 2d displays the radial dimensions of the main concentric components of the cable, obtained from the optimization process. The increase in R_f with power is due to the increase in the number of MgB_2 wires that must be wound around the former outer circumference. Even though R_f widens, the outer radial dimension of the cable tends to decrease with power, as the algorithm chooses to limit the external surface of the cryostat to reduce the thermal inputs affecting the cooling costs. Between 1 GW and 3 GW, this trend is explained by a shrinkage of the insulation thickness alone. Indeed, if the same voltage level does not vary, the amount of insulation required remains the same, thus the thickness of the insulating layer reduces as its inner radius rises. The increase of the insulation inner radius is proportional to power as a result of the increase in the underlaying radius of the former R_f. Then, passing from 0.75 GW to 1 GW, there is also a notable reduction in the thickness of the annular duct, which in turn determines smaller inner radii of the cryostat. Most probably, the 0.75 GW case presents the largest t_{an} value to comply the fluid-dynamic constraints of LN_2, which must handle more heat than the other cases. From the 1 GW case onwards, the optimized t_{an} value corresponds to the lower boundary imposed by the user for this analysis (1 cm).

Then, readers may observe that the cryostat in the 1 GW case features a slightly larger outer radius than the higher power cases, attributed to a thicker insulation layer. This difference helps to account for the minimal deviation from the increasing trend in Fig. 2c between 1 and 3 GW of, occurring at the 1.25 GW case. Indeed, the 1.25 GW scenario exhibits 1.3% lower total operating costs compared to the 1 GW case. This disparity may be attributed to the slightly higher losses in the 1 GW case, primarily from the cryostat, owing to its larger external surface. Such modest deviation from the overall trend may also fall within the reasonable tolerance of the adopted stochastic algorithm.

IV. Conclusions

This work proposes a tool to determine the optimal configuration of DC power transport cables realized with MgB_2 wires,

that minimizes the total cost of the cable system. The model is adapted from the OSCaR code. Appropriate assumptions are made to implement the novel cable design and relate its features to costs and operating constraints. An accurate fluid-dynamic numerical model is implemented as an upgrade of the previous one, to estimate the properties of the cryogenic fluids selected.

The tool is particularly suitable for carrying out parametric analyzes on the line operating conditions, the properties, and the cost of single cable components, and the applied electrical or fluid-dynamic constraints. As a case study, the results of the optimization process varying the power delivered through the line are shown. The optimized radial encumbrance of the cable is reduced as the power increases, although the former radius progressively increases. This allows the external surface of the cryostat to be narrowed, thus limiting the corresponding thermal inputs into the cable, which constitute the main loss contribution. Indeed, operating costs for cable cooling are double the total capital costs, over a 40-year lifetime. The cost of MgB_2 wires is almost negligible, while the capital costs for the cryostat and cabling are significant; dedicated parametric analyzes are envisaged to assess how to minimize these cost indexes.

The proposed approach can be easily adapted to consider different cable designs and optimizable variables, as well as other cryogenic fluids, thermal inputs and cost indexes omitted here.

REFERENCES

[1] A. Ballarino *et al.,* "Status of MgB_2 wire and cable applications in Europe," J. Phys.: Conf. Ser., Vol. 871, p. 012098, 2017.

[2] A. Ballarino *et al*., "The BEST PATHS Project on MgB_2 Superconducting Cables for Very High Power Transmission," IEEE Trans. On. Appl. Supercond., Vol. 26, no. 3, Apr. 2016.

[3] A. Ballarino *et al*., "Development of superconducting links for the Large Hadron Collider machine," Supercond. Sci. Technol., Vol. 27, Mar. 2014, Art. no. 044024.

[4] V.V. Kostyuk *et al.,* "Cryogenic design and test results of 30-m flexible hybrid energy transfer line with liquid hydrogen and superconducting MgB_2 cable," Cryogenics, Vol. 36, pp. 34 – 42, Dec. 2014.

[5] P.M. Grant, "The SuperCable: Dual Delivery of Chemical and Electric Power," IEEE Trans. On. Appl. Supercond., Vol. 15, no. 2, pp. 1810 – 1813, Jun. 2005.

[6] S. Yamada *et al*, "Study on 1 GW class hybrid energy transfer line of hydrogen and electricity," J. Phys.: Conf. Ser., Vol. 97, 2008, Art. no. 012167.

[7] V.S. Vysotsky et al., "Energy transfer with hydrogen and superconductivity – the review of the first experimental results," Physics Procedia, Vol. 65, pp. 299 – 302, 2015.

[8] T. Nakayama et al., "Micro Power Grid System With SMES and Superconducting Cable Modules Cooled by Liquid Hydrogen," IEEE Trans. On. Appl. Supercond., Vol. 19, no. 3, pp. 2062 – 2065, Jun. 2019.

[9] Y. Zebang et al., "Feasibility and Economical Analysis of the Superconducting Cable and Hydrogen Hybrid Transmission Gallery," Proceedings of 2020 IEEE International Conference on Applied Superconductivity and Electromagnetic Devices (ASEMD), Tianjin, China, Oct. 16-18, 2020.

[10] G. Escamenez, "AC losses in superconductors: a multi-scale approach for the design of high current cables. Electric power," Ph.D. Dissertation, Université Grenoble Alpes, France, 2016.

[11] Y. Nikulshin *et al.,* "Effect of magnetic sheath on filament AC losses and current distribution in MgB2 superconducting wires: numerical analysis," Supercond. Sci. Technol., Vol. 32, 2019, Art. no. 075007.

[12] Y. Nikulshin *et al.,* "Monel Contribution to AC Losses in MgB_2 Wires in Frequencies Up To 18 kHz," IEEE Trans. Appl. Supercond., vol. 28, no. 8, Dec. 2018, Art. no. 6200906.

[13] F. Grilli *et al*., "Numerical modeling of MgB_2 conductors for high power AC transmission," Physica C: Superconductivity and its Applications, Vol. 504, pp. 167 – 171, Sept. 2014.

[14] D. Politano *et al.,* "Technical and economical assessment of HTS cables," IEEE Trans. Appl. Supercond., vol. 11, no. 1, pp. 2477–2480, Mar. 2001.

[15] L. Ren *et al.,* "Techno-Economic feasibility study on HTS power cables," IEEE Trans. Appl. Supercond., vol. 19, no. 3, pp. 1774–1777, Jun. 2009.

[16] W. Yuan *et al*., "Economic feasibility study of using high temperature superconducting cables in U.K.'s electrical distribution networks," IEEE Trans. Appl.Supercond., vol. 28, no. 4, Jan. 2018, Art. no. 5401505.

[17] P. C. Ferran, "Economical study of electric power transmission with superconducting lines for HVDC systems," Ph.D. dissertation, Escola Tècnica Superior d'Enginyeria Industrial de Barcelona, Spain, 2021.

[18] Z. Yu *et al.,* "Feasibility and economical analysis of the superconducting cable and hydrogen hybrid transmission gallery," in Proc. IEEE 2020 Int. Conf. Appl. Supercond. Electromagn. Devices, pp. 1 – 2, 2020.

[19] S. H. Venuturumilli *et al*., "Superconducting cables-network feasibility study work package 3," 2017. [Online]. Available: *https://www.western-power.co.uk/downloads-view-reciteme/2152*

[20] R. Guarino *et al*., "Technical and economic feasibility study of high-current HTS bus bars for fusion reactors," Physica C: Supercond. Appl., vol. 592, 2022, Art. no. 1353996.

[21] A. Morandi, "HTS dc transmission and distribution: concepts, applications and benefits," Supercond. Sci. Technol., Vol. 28, Oct. 2015, Art. no. 123001.

[22] S. Kloppel *et al*., "Thermo-hydraulic and economic aspects of long length high-power MgB2 superconducting cables," Cryogenics, vol. 113, Oct. 2020, Art. no. 103211.

[23] A. Musso *et al.,* "OSCaR: A Cost Analysis of HTS Coaxial Cables With a Novel Optimization Method," IEEE Trans. Appl. Supercond., vol. 33, no. 5, Aug. 2023, Art. no. 4803516.

[24] A. Musso *et al.,* "A method to quantify technical-economic aspects of HTS electric power cables," IEEE Trans. Appl. Supercond., vol. 32, no. 9, Dec. 2022, Art. no. 4803516.

[25] MATLAB. Version 2020a, The Math Works Inc., Natick, Massachusetts, United States, 2020.

[26] A. Ballarino, "Alternative Design Concepts for Multi-Circuit HTS Link Systems," IEEE Trans. Appl. Supercond., vol. 21, no. 3, pp. 980 – 983, Jun. 2011.

[27] D. S. Kwag *et al.,* "A study on the composite dielectric properties for an HTS cable," IEEE Trans. Appl. Supercond., vol. 15, no. 2, pp. 1731–1734, Jun. 2005.

[28] H. Takahashi *et al.,* "Dielectric Properties of 500 m Long HTS Power Cable," IEEE Trans. Appl. Supercond., vol. 15, no. 2, pp. 1767 – 1770, Jun. 2005.

[29] J. Choi *et al.,* "A study on insulation characteristics of laminated polypropylene paper for an HTS cable," IEEE Trans. Appl. Supercond., vol. 20, no. 3, pp. 1280 – 1283, Jun. 2010.

[30] S. H. Kim *et al.,* "Electrical Insulation Characteristics of PPLP as a HTS DC Cable Dielectric and GFRP as Insulating Material for Terminations," IEEE Trans. Appl. Supercond., vol. 22, no. 3, Jun. 2012, Art. no. 7700104.

[31] H. Kim *et al.,* "The Basic Dielectric Characteristics of Insulating Materials for HTS DC Cable System," IEEE Trans. Appl. Supercond., vol. 26, no. 3, Apr. 2016, Art no. 7701104.

[32] W. Kim *et al.,* "Comparative Study of Cryogenic Dielectric and Mechanical Properties of Insulation Materials for Helium Gas Cooled HTS Power Devices," IEEE Trans. Appl. Supercond., vol. 27, no. 7, Jun. 2017, Art no. 7700605.

[33] W. Pi *et al.,* "Insulation design and simulation for three-phase concentric high-temperature superconducting cable under 10-kV power system," IEEE Trans. Appl. Supercond., vol. 29, no. 2, Mar. 2019, Art no. 7700104.

[34] C. Peng *et al.,* "Insulation Characteristics of Dielectric Material for CD HTS Cable," IEEE Trans. Appl. Supercond., vol. 29, no. 2, Mar. 2019, Art. no. 7700405.

[35] D. Kottonau *et al.,* "Design comparisons of concentric three-phase HTS cables," IEEE Trans. Appl. Supercond., vol. 29, no. 6, Sep. 2019, Art no. 5401508.

[36] L. Trevisani *et al*., "Long distance renewable-energy-sources power transmission using hydrogen-cooled MgB_2 superconducting line," Cryogenics, Vol. 47, no. 2, pp. 113 – 120, Feb. 2007.

[37] M. N. Wilson, "Superconducting Magnets", Oxford University Press, 1983.

[38] X. Zhihan, and F. Grilli. "Modelling ac ripple currents in HTS coated conductors" Supercond. Sci. Technol., vol. 28, n. 10, Art. no. 104002, 2020.

[39] M. Tropeano *et al.,* "MgB_2 round wires for the high power superconducting cable demonstrator in Best Paths project", 2017. [Online]. Available : *https://indico.cern.ch/event/659554/contributions/2709608/attachments/1527414/2388832/4MO2-06_Matteo_Tropeano_Room_34.pdf*.

[40] C. E. Bruzek *et al.,* "Cable Conductor Design for the High-Power MgB_2 DC Superconducting Cable Project of BEST PATHS", IEEE Trans. Appl. Supercond. vol .27, no. 4, 2017.
[41] H. E. Knoepfel, "Magnetic Fields: A Comprehensive Theoretical Treatise for Practical Use", Wiley & Sons, Inc., 2000.
[42] G. Angeli *et al.*, "Development of Superconducting Devices for Power Grids in Italy: Update About the SFCL Project and Launching of the Research Activity on HTS Cables," IEEE Trans. Appl. Supercond., vol. 27, no. 4, Jun. 2017, Art. no. 5600406.
[43] L. Savoldi *et al.,* "The 4C code for the cryogenic circuit conductor and coil modeling in ITER," Cryogenics, vol. 50, no. 3, pp. 167 – 176, Mar. 2010.
[44] R. T. Jacobsen, S. G. Penoncello, and E. W. Lemmon, "Thermodynamic Properties of Cryogenic Fluids," The International Cryogenics Monograph Series, New York, NY, USA: Plenum, 1997.
[45] Thermophysical Properties of Fluid Systems," National Institute of Standards and Technology (NIST). [Online]. Available : *http://webbook.nist.gov/chemistry/fluid/*
[46] R. Zuijderduin, "Integration of high-Tc superconducting cables in the dutch power grid of the future," Ph.D. dissertation Delft Univ. of Technology, Delft, The Netherlands, 2016.
[47] A. Preuß, "Development of high-temperature superconductor cables for high direct current applications," Ph.D. dissertation, KIT Scientific Publishing, Institut für Technische Physik (ITEP), Germany, 2022.
[48] K. Reddi *et al*., "Impact of hydrogen refueling configurations and market parameters on the refueling cost of hydrogen," International Journal of Hydrogen Energy, vol. 42, no. 34, pp. 21855-21865, Aug. 2017.
[49] [Online]. Available : *https://www.marketindex.com.au/copper*